plasma

MDPI

Article

Thermal Plasma Spheroidization and Characterization of Ti6Al4V Powders Using DC Plasma Technology

Pierpaolo Iovane [1,*], Sabrina Portofino [1], Carmela Borriello [1], Giuseppe Pandolfi [1], Anna De Girolamo Del Mauro [2], Nicola Fedele [3] and Sergio Galvagno [1]

[1] Laboratory Smart Components and Systems for Sustainable Manufacturing, Division Technologies and Materials for Sustainable Manufacturing Industry, Department for Sustainability, Italian National Agency for New Technologies, Energy and Sustainable Economic Development (ENEA), 80055 Portici, Italy; sabrina.portofino@enea.it (S.P.); carmela.borriello@enea.it (C.B.); giuseppe.pandolfi@enea.it (G.P.); sergio.galvagno@enea.it (S.G.)

[2] Laboratory Innovative Devices, Division Solar Photovoltaics, Department for Energy Technologies and Renewable Sources, Italian National Agency for New Technologies, Energy and Sustainable Economic Development (ENEA), 80055 Portici, Italy; anna.degirolamo@enea.it

[3] Laboratory Regenerative Circular Bioeconomy, Division Sustainable Agrifood Systems, Department for Sustainability, Italian National Agency for New Technologies, Energy and Sustainable Economic Development (ENEA), 80055 Portici, Italy; nicola.fedele@enea.it

* Correspondence: pierpaolo.iovane@enea.it; Tel.: +39-081-772-3297

Abstract

Titanium alloy Grade 5 (Ti6Al4V) is a widely used material for aerospace components and biomedical implants due to its excellent combination of strength, low density, corrosion resistance and biocompatibility. Additive manufacturing (AM) technologies, such as Laser Powder Bed Fusion (LPBF) and Electron Beam Melting (EBM), could contribute to the manufacturing of high-performance Ti6Al4V components with complex geometries at reduced waste material and costs, but require powders with controlled morphology and flowability. Plasma Spheroidization is a key process for producing spherical titanium alloy powders suitable for AM; however, Direct Current (DC) thermal plasma is generally optimized for fine particle sizes. This study investigated the spheroidization of irregular Ti6Al4V powders (45–106 μm) through the optimization of DC thermal plasma processing parameters with the aim of extending its applicability to coarser powders. Particular attention was dedicated to particle size classification before and after plasma treatment. Pre-treatment sieving was found to be the most effective strategy for enhancing spheroidization and powder quality, while post-treatment classification improved the homogeneity of the final product. The resulting products were characterized by X-ray diffraction, morphological analysis, and flowability testing. High circularity powders (>0.7) with improved flowability (<30 s/50 g) were successfully obtained. The results demonstrate the potential of DC thermal plasma processing for producing coarser Ti6Al4V powders suitable for AM applications.

Keywords: plasma; titanium alloy; spheroidization; additive manufacturing

Check for updates

Academic Editors: Filipe Vaz and Andrey Starikovskiy

Received: 10 July 2026
Revised: 7 August 2026
Accepted: 21 August 2026
Published: 1 September 2026

Copyright: © 2026 by the authors. Licensee MDPI, Basel, Switzerland. This article is an open access article distributed under the terms and conditions of the Creative Commons Attribution (CC BY) license.

1. Introduction

Titanium alloy Grade 5, commonly known as Ti-6Al-4V, is widely used in several sectors due to its excellent combination of strength, low density, corrosion resistance, and biocompatibility. This material is a combination of α and β titanium phases containing approximately 6% aluminum (an α-phase stabilizer) and 4% vanadium (a β-phase stabilizer), which together provide a balanced and versatile microstructure with excellent mechanical

properties. The material exhibits a high strength-to-weight ratio, with mechanical strength comparable to some steels while being about 40% lighter, maintaining good mechanical performance at elevated temperatures, up to around 400 °C. The alloy also demonstrates excellent resistance to corrosion in a wide range of environments, including marine, chemical, and physiological conditions, and good fatigue strength and fracture toughness, making it suitable for highly stressed structural components.

This alloy is extensively used in aerospace applications such as airframe structures, turbine components, and fasteners, due to its strength-to-weight advantages. In the biomedical field, Ti-6Al-4V is commonly employed for implants and prosthetics because of its biocompatibility and ability to osseointegrate. Furthermore, its corrosion resistance and biocompatibility, combined with good weldability and melting behavior, make it particularly suitable for metal AM processes. Its ability to form stable and homogeneous melt pools under high-energy heat sources enables the production of fully dense, low-defect, high-performance parts with complex geometries and low residual stresses [1]. The conventional methods (such as casting, forming, machining and powder metallurgy processes) are still preferred for large-scale production and are well-established processes, but they have several weaknesses, such as poor machinability and rapid tool wear, high production costs for complex controlled processes, high waste material and difficulty in producing complex geometries; so, AM processes are increasingly favored to overcome these difficulties [2].

The most common additive manufacturing techniques for Ti-6Al-4V are Laser Powder Bed Fusion (LPBF) and Electron Beam Melting (EBM). Both processes rely on the selective melting of successive thin layers of titanium alloy powder spread over a powder bed, using either a focused laser beam or an electron beam as the energy source. The production of high-quality components requires the use of highly spherical powders with carefully controlled particle size distribution, morphology, and physicochemical properties. Such powder characteristics are essential for achieving adequate flowability and high packing density, which facilitate the formation of thin, uniform powder layers, ensure homogeneous melting during processing and minimize the occurrence of defects in the final part. Typically, LPBF processes employ powders with particle sizes ranging from 15 to 45 μm, while EBM utilizes coarser powders, generally within the 45–106 μm size range [3,4]. To ensure high flowability, uniform layer deposition and consistent melting behavior, plasma-spheroidized or gas-atomized powders are typically used for the manufacturing process [5].

Each atomization process has advantages and disadvantages in terms of the form, shape, and complexity of the process. Water atomization is widely used for powder production; it can produce irregular, rounded particles from ingots in the 45–106 μm range with high production rates, but an additional process of water removal and irregular particle shape are necessary [6]. Actually, water atomization is rarely used for titanium because molten titanium reacts aggressively with water at high temperatures, causing explosions and severe oxidation. Gas atomization is the most widespread technology, but it can present different drawbacks, such as a large number of satellites (which negatively influence the flowability of the particles), irregular particle shape and low sphericity together with gas entrapments [7]. The use of this process for titanium powder production is constrained by the high chemical reactivity of titanium with process gases (particularly nitrogen).

The Plasma Rotating Electrode Process (PREP) enables the production of high-purity, near-spherical titanium alloy powders within the 50–350 μm size range. However, achieving particle sizes below 106 μm presents significant challenges, as it necessitates substantially increasing the billet rotation speed—often exceeding 30 000 rpm—posing operational and mechanical limitations [8]. Plasma atomization (PA) can generate very good sphericity and fewer satellite particles from wires, but the high cost of Ti limits its use [7].

Plasma spheroidization (PS) is a new advanced powder-processing technique used to produce spherical titanium alloy powders with high purity and controlled particle size, which are essential for additive manufacturing and powder metallurgy applications [9,10]. In this process, irregularly shaped titanium alloy particles, injected into a high-temperature plasma jet, are molten and solidify into near-perfect spheres by surface tension forces during flight in a cooling chamber.

Different researchers have studied the spheroidization of Ti6Al4V using different feedstocks and inductively coupled plasma (ICP) with the aim of producing fine powders with a narrow particle size distribution (PSD) of 15–45 μm for LPBF applications [11–15]. For example, Huang et al. 2026 [16] introduced a novel approach for the production of spherical Ti6Al4V by ICP plasma starting from scraps (<150 μm), producing fine powders (d_{50} = 58 μm) with 2.09 g·cm^{-1} of apparent density, 2.70 g·cm^{-1} of tapped density and 24 s/50 g of flowability.

Direct Current (DC) thermal plasma is an emerging approach in the context of PS, particularly for the production of titanium alloy powders. Its relatively low cost and potential for industrial scalability make it an attractive alternative to more established techniques such as ICP. In any case, while the traditional plasma processes are usually optimized for the production of fine powders, the obtainment of spherical powders over a broad particle size range for additive manufacturing applications is still challenging.

This paper presents the results of an experimental work conducted on irregular Ti6Al4V powders (45–106 μm) aimed at identifying the optimal DC thermal plasma processing parameters for producing coarse spherical powders. X-ray diffraction, morphological and flowability analyses were performed to characterize reagents and products. The collected results were compared with data available in the literature to identify the potential use of the produced spherical powders in AM technologies.

2. Materials and Methods

Commercial titanium alloy (Ti6Al4V) powders (METCO 4030C) provided by OERLIKON METCO (Cusago, MI, Italy) were used for experimental work.

The raw powders were processed using a custom-designed DC thermal plasma system installed at ENEA Research Centre of Portici.

The system consists of a powder feeder system (GTV PF 2/2; GTV Verschleißschutz GmbH, Luckenbach, Germany), a DC non-transferred plasma torch (Praxair Surface Technologies, F4 model, Fornovo di Taro, PR, Italy), a power supply (GTV 800 A, GTV Verschleißschutz GmbH, Luckenbach, Germany), a cyclone/bag filter, and a dry scroll pump for vacuum. The plasma operates under a light vacuum (up to 80 kPa). The torch consists of a standard water-cooled V-shaped tungsten cathode and an 8 mm copper/tungsten anode nozzle supplied by Praxair Surface Technologies. It is mounted at the top of a jacketed cylindrical stainless-steel reactor with an inner diameter of 13 cm and a length of 185 cm, cooled with circulating cold water. The reactor is equipped with a collection tank in which the produced powders and any unreacted materials are collected. At the top of the reactor, a nozzle injects the powder directly into the plasma flame. The nozzle has an inner diameter of 2.4 mm and is positioned approximately 2 cm away from the center of the flame. A positioning ring at the base of the torch ensures correct alignment and fixes the powder injection angle at 75° for all experiments. Further details of the plant and experimental set-up have been reported elsewhere [17].

The tests were performed by varying the current value (in the 290–750 A range) on the programmable logic controller (PLC) to achieve the desired power; the voltage value was adjusted accordingly by the power supply connected to the DC plasma torch, and ranged

from 36 to 46 V. The plasma processing parameters investigated in the experiments are summarized in Table 1.

Table 1. Process parameters for Ti6Al4V powder.

Parameters	Values
Arc power (kW)	15–21–31
Net plasma power (kW)	7.9–12.2–18.5
Ar/H_2 main gas (slpm)	47
He secondary gas (slpm)	8
Ar/H_2 carrier powder (slpm)	3
Feed rate (kg/h)	1.2

Arc power represents the total electrical power supplied to the system, whereas the net plasma power corresponds to the effective power delivered to the plasma jet. The net power is calculated by subtracting the thermal power losses dissipated through the torch's water-cooling system from the total supplied power.

Both the main gas and carrier powder flows consist of an argon (Ar)–hydrogen (H_2) mixture (3% v/v in H_2), corresponding to the maximum allowable hydrogen concentration under standard safety regulations of our Research Center. This mixture was utilized to enhance the efficiency of the DC plasma spheroidization process. The addition of H_2 significantly improves the thermal conductivity and enthalpy of the plasma jet due to the high dissociation and recombination energy of the molecules. As a result, heat transfer to the in-flight powder particles is improved, promoting complete melting and optimal spheroidization. Furthermore, H_2 acts as a strong reducing agent, effectively removing surface oxide layers and suppressing oxidation during processing. Although H_2 can interact with titanium, its chemical affinity for this material is lower than that of oxygen.

The produced powders were obtained by combining those collected from both the collection tank and the cold walls of the reactor chamber. The resulting powders were cleaned using an in-house method consisting of ultrasonic treatment in ethanol (37 kHz, 20 min). After ultrasonication, the nanoparticles that eventually formed were removed once settled at the top of the liquid surface.

A sieve machine (Retsch AS basic 200, Retsch GmbH, Haan, Germany; distributed in Italy by Verder Scientific Italia, Pedrengo, BG, Italy) was used both for the raw material and the produced powders, while their characterization was performed with the following methods.

Morphological analyses of the samples were carried out by a scanning electron microscope (SEM, Carl ZEISS LEO 1530 SMT GmbH, Oberkochen, Germany) equipped with a filament of tungsten at 4 kV and working under high vacuum conditions. The SEM micrographs were used and further processed to measure the particles' dimensions. Image processing and calculation were performed using an image editor ("ImageJ" Software, version 1.54 g, NIH and LOCI, Wisconsin, WI, USA) to determine mean circularity and spheroidization. The circularity factor, C, is given by the formula:

$$C = 4\pi A/P \quad (1)$$

where P is the perimeter (μm) and A is the area (μm^2), both determined from the ImageJ software, which directly gives both the circularity value for each counted particle and the mean circularity value for the whole sample. C values close to 1 indicate near-perfect circular particles, while C values close to 0 demonstrate increasingly irregularly shaped particles. The analysis for the determination of such a shape factor is conducted on an average of 1000 particles. The guidelines provided by Cordova et al. [18] recommended

that the circularity factor of the recycled powders needs to be as close to 1 as possible, or at least >0.7. For this reason, the degree of spheroidization is defined as the percentage of particles whose circularity was higher than 0.7.

The particle size distribution (PSD) was calculated using a Laser Diffraction MICROTRAC MRB SYNC 3R equipped with system dry dispersion TURBOSYNC (Microtrac MRB, Haan, Germany, supplied by VERDER Scientific S.r.l., Pedrengo, BG, Italy). An additional parameter can be used in this analysis to quantify the distribution width, defined by Equation (2):

$$\text{SPAN} = (d_{90} - d_{10})/d_{50} \quad (2)$$

where d_{90} represents the point at which the cumulative (from 0 to 100%) undersize particle size distribution reaches 90%, as for d_{50} and d_{10}. This parameter provides a comprehensive description of the powder size distribution width before and after plasma spheroidization. The use of this metric and its calculation are standard practices across the material characterization industry, fully integrated into major analytical instrumentation guidelines (such as Microtrac MRB (Haan, Germany), Malvern Panalytical Ltd. (Worcestershire, UK) and Horiba systems (Kyoto, Japan)) and aligned with global standardization frameworks).

Phase identification of these samples was performed by X-ray diffraction (XRD), using an Aeris compact X-ray diffractometer (Malvern Panalytical, Lissone, MB, Italy; supplied by Alfatest S.r.l., Cernusco sul Naviglio, MI, Italy), operated at 40 kV and 15 mA and equipped with a Cu-anode X-ray tube. XRD patterns were collected in the 5–80° 2θ range, with a step size of 0.05° and an acquisition time of 5 s per step. Phase identification was carried out by comparison with standard Joint Committee on Powder Diffraction Standards (JCPDS) cards, namely α-Ti (JCPDS No. 44-1294) and β-Ti (JCPDS No. 44-1288), commonly adopted for Ti-6Al-4V alloys.

Oxygen, nitrogen and hydrogen concentrations, which strongly influence the properties of Ti6Al4V powder, were measured by an ELTRA combustion analyzer ONH (VERDER Scientific S.r.l., Pedrengo, BG, Italy) that uses the inert gas fusion technique for the elemental analysis of inorganic sample materials. Its internal IR sensor and TCD were used to determine oxygen as carbon dioxide, and nitrogen/hydrogen contents of the spheroidized powder, respectively. The analyses were carried out under ASTM specifications.

The flowability and the apparent density of the powders were evaluated by using a POWDERFLOW kit (Carpenter Additive, Philadelphia, PA, USA; supplied by LPW South Europe, San Pietro Mosezzo, NO, Italy). According to the standard protocol (ASTM B213), 50 g of powder is timed passing through the funnel, and the result of the flowability is given as s/50 g. ASTM B212 method is used instead to measure the apparent density (a relationship that links the mass of powder that fills a die cavity and the calibrated volume of that cavity).

3. Results and Discussion

The preliminary tests were conducted on as-received commercial powders by varying the plasma power and keeping the other parameters constant (gas flow rate, carrier powder and feed rate). The processing conditions are summarized in Table 2.

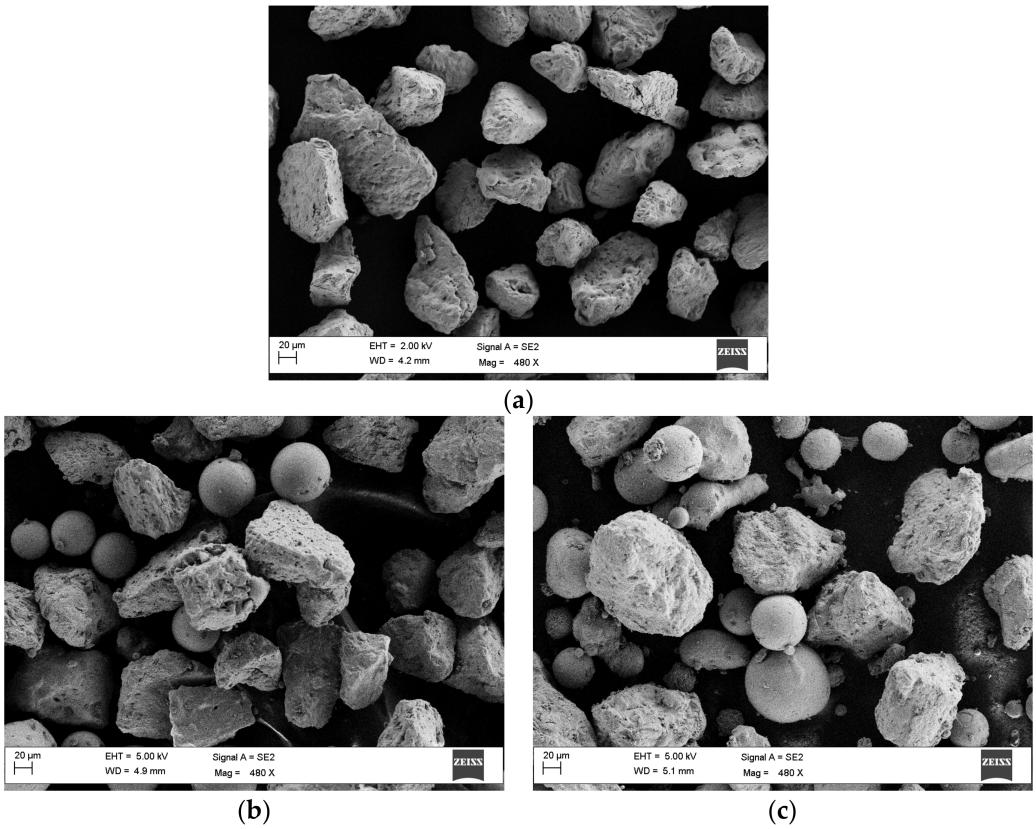
Table 2 also reports the particle size distribution of the Ti6Al4V powders before and after plasma treatment. The commercial raw powder shows d_{10}, d_{50}, and d_{90} of 63.3, 90.2 and 137.8 μm, respectively. After plasma processing, both preliminary tests showed a reduction in the median particle size (d_{50}), from 90.2 μm to 77.5 μm (test P1) and 73.8 μm (test P2). A similar decrease was observed for both d_{10} and d_{90}, suggesting a general shift in the particle size distribution toward finer particles. Test P1 also led to a slight reduction in SPAN (0.7), indicating a narrower particle size distribution compared with

the raw powder, whereas test P2 showed a higher SPAN (0.9), corresponding to a broader distribution despite the lower median particle size.

Table 2. Comparison between two tests of plasma spheroidization of Ti6Al4V powder.

Preliminary Test	Net Plasma Power (kW)	Carrier Powder (slpm)	Feed Rate (kg/h)	d_{10} (µm)	d_{50} (µm)	d_{90} (µm)	SPAN
Raw	-	-	-	63.3	90.2	137.8	0.8
P1	12.2	3	1.2	57.6	77.5	114.6	0.7
P2	18.5	3	1.2	51.7	73.8	119.8	0.9

During plasma spheroidization, the injected particles absorb energy from the plasma, and when the absorbed energy is sufficient, the particles melt. Exiting the plasma plume, the molten particles cool rapidly, and surface tension forces drive their transformation into a spherical shape during solidification. However, the wide particle size distribution of the raw material led to heterogeneous properties of the feed. Larger particles require higher energy to achieve complete melting, whereas finer particles melt rapidly and may even partially evaporate. Consequently, different particle fractions experience different spheroidization degrees across the batch, reducing the overall process efficiency. In addition, a wider particle size distribution in the feeding produces different trajectories and residence times in the plasma, affecting process uniformity. For these reasons, the spheroidization process proved to be ineffective under these conditions, as shown by SEM images (Figure 1).



(**a**)

(**b**) (**c**)

Figure 1. Raw material (**a**), P1 (**b**), and P2 (**c**) samples after treatment at 480× magnification.

Under the process conditions explored, particles with diameters greater than 90 microns are difficult to spheroidize, even at high power, primarily because they require significantly higher energy inputs or longer residence times to fully melt [19].

Moreover, particle fraction on the cold walls increases from 30% w/w to 70% w/w when power increases from 12.2 to 18.5 kW. Powder deposition on the reactor walls is mainly caused by particle inertia, reduced gas velocity near the wall and rapid solidification upon contact with the cooler surface. When the particles deviate from the main gas stream, they are more likely to impact the wall, where the lower temperature promotes the adhesion of partially molten particles. Thermal gradients and local flow recirculation may further enhance wall deposition.

The low spheroidization degree of the powders observed in the preliminary tests can be mainly attributed to the wide particle size distribution of the feedstock. Therefore, a new set of experiments was carried out using a sieved fraction of the starting material, setting the arc power also below 21 kW (Table 3).

Table 3. Secondary tests for sieved Ti6Al4V powder.

Test	Net Plasma Power (kW)	Carrier Powder (slpm)	Feed Rate (kg/h)	d_{10} (μm)	d_{50} (μm)	d_{90} (μm)	SPAN
Raw (sieved)	-	-	-	64.2	86.6	128.2	0.7
A test—wall	12.2	3	1.2	55.5	76.0	115.6	0.8
A test—tank		3	1.2	64.9	86.3	124.8	0.7
C test—wall	7.9	3	1.2	40.6	60.8	91.8	0.8
C test—tank		3	1.2	52.3	69.2	101.1	0.7

The raw material exhibited a median particle size (d_{50}) of 90.2 μm (Table 2), which decreased to 86.6 μm after the removal of larger and finer particles, confirming the effectiveness of the sieving process in narrowing the particle size distribution (SPAN decreased from 0.8 to 0.7).

The powders collected on the walls exhibited a significant reduction in particle size in both tests. This effect is probably governed by the fluidodynamic characteristics of the DC plasma jet. Finer droplets are more easily entrained by the plasma flow and deposited on the colder chamber walls, where rapid quenching preserves their smaller size and leads to broader PSDs (higher SPAN values). Conversely, larger particles retain sufficient momentum to remain along the jet axis and are therefore preferentially collected in the tank [20,21]. The evolution of the median particle size d_{50} may be strongly influenced by the plasma torch power when operating with an Ar-H_2 gas mixture. At a lower power input of 7.9 kW, the d_{50} of the processed powder shows a significant reduction compared to the raw material. This phenomenon may be attributed to in-flight melting behavior, feedstock agglomerate merging, and fine-fraction evaporation [12,14]. At this lower power level (7.9 kW), the thermal energy density is insufficient to fully remelt and support in-flight particle growth, shifting the overall size distribution toward lower values.

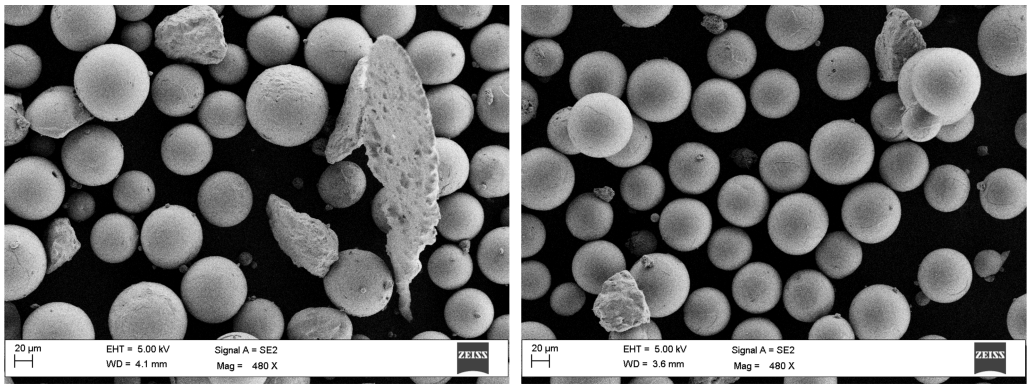
In all tests, the SPAN value remained below 1, indicating a narrow and highly uniform PSD with a limited presence of both fine or coarse particles.

The best results in terms of spheroidization were obtained in these tests and the produced powders were analyzed by SEM images (Figure 2).

After plasma treatment, most particles exhibit a nearly spherical morphology, even if a small fraction of irregular particles and a fused agglomerate are still present in test A (12.2 kW). This result motivated further experiments at lower plasma power (7.9 kW) to reduce agglomeration while preserving the spheroidization efficiency.

To better assess the influence of the process parameters on the degree of spheroidization, the powders collected by the walls and the tank were purified separately for each test,

subsequently combined, and sieved in the 45–90 µm range (see SEM images of the different fractions in Figure 3).

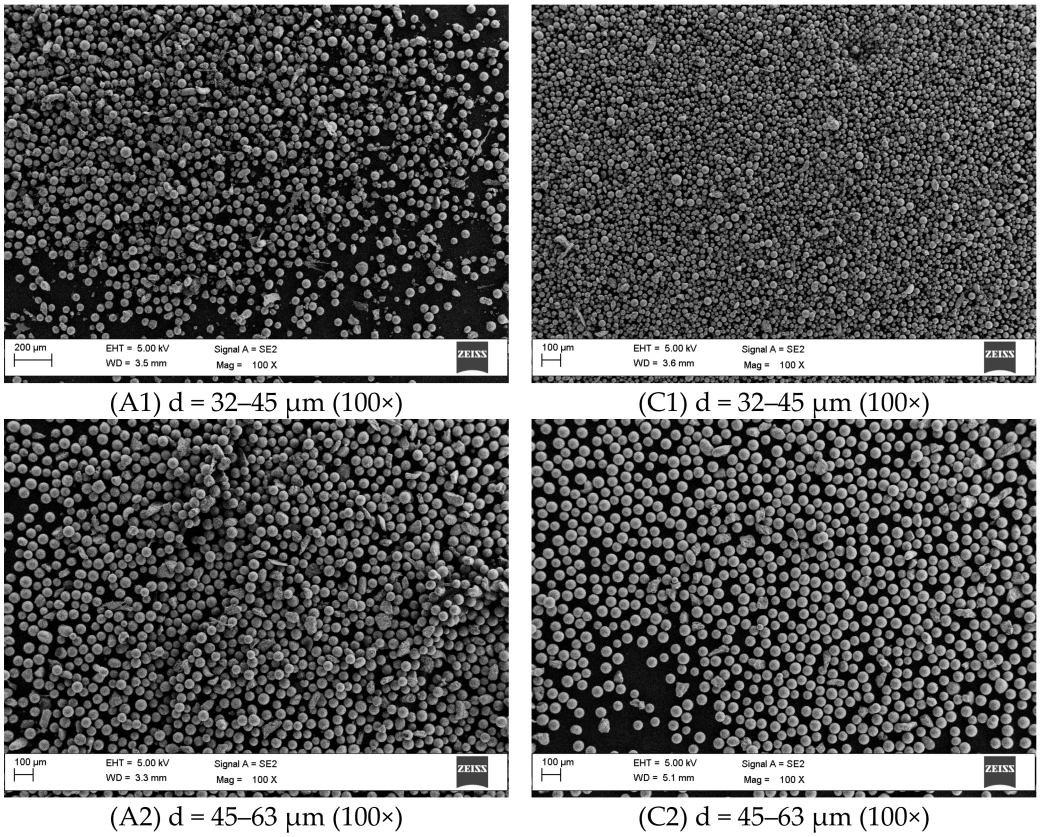


(**a**) (**b**)

Figure 2. A (**a**) and C (**b**) samples (powders collected from both the reactor walls and the collection tank) after plasma treatment at 480× magnification.

SEM images confirm the effectiveness of the DC plasma spheroidization treatment. In fact, they show a high degree of spheroidization in the 32–63 µm size range for both samples. In the 63–90 µm fraction, spheroidization slightly decreases, and the presence of unreacted material increases for test A (12.2 kW), whereas sample C maintains a high degree of spheroidization.

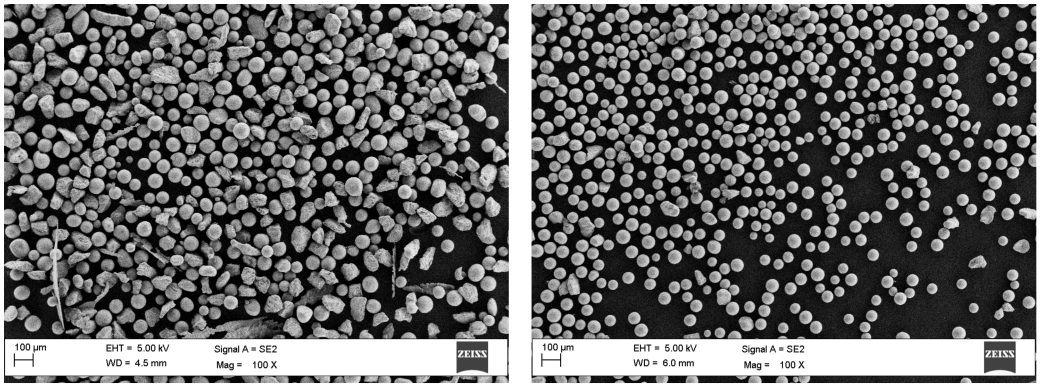
The predominance of particles with a spherical morphology and the absence of satellites ensure high powder flowability, enabling more uniform layer deposition and a good packing density in 3d printing.



(A1) d = 32–45 µm (100×) (C1) d = 32–45 µm (100×)

(A2) d = 45–63 µm (100×) (C2) d = 45–63 µm (100×)

Figure 3. *Cont.*



(A3) d = 63–90 µm (100×) (C3) d = 63–90 µm (100×)

Figure 3. SEM images of samples A and C after purification and classification into different particle size ranges (A1 and C1 32–45 µm; A2 and C2 45–63 µm; A3 and C3 63–90 µm).

The circularity and spheroidization degree were adopted as the primary shape factor parameters, and the corresponding results are reported in Table 4.

Table 4. Powder characteristics (mean circularity and spheroidization degree) for Ti6Al4V spheroidized powder.

	Net Plasma Power (kW)	Mean Circularity	Spheroidization Degree (%)
A not sieved	12.2	0.6	50.4
A1 (32–45 µm)		0.6	40.7
A2 (45–63 µm)		0.8	71.0
A3 (63–90 µm)		0.7	58.2
C not sieved	7.9	0.8	70.6
C1 (32–45 µm)		0.7	61.5
C2 (45–63 µm)		0.8	77.8
C3 (63–90 µm)		0.8	90.1

The powders processed exhibited consistently superior morphological characteristics in test C than those processed in test A; in fact, the powders exhibited higher circularity and a greater degree of spheroidization when they were processed at 7.9 kW than at 12.2 kW. The higher spheroidization degree observed at the lower nominal power may indicate that 7.9 kW was closer to the optimal processing window for the specific Ti powder fraction investigated. In this case, the nominal torch power did not necessarily correspond to a higher effective energy transfer to the particles, since spheroidization is governed not only by power, but also by PSD, injection conditions, plasma stability, residence time, and the actual thermal interaction between the plasma jet and the powder.

The samples C2 and C3 (45–90 µm range) showed the best results, indicating that this combination of processing power and particle size fraction is the most effective for producing highly spherical Ti6Al4V powders suitable for additive manufacturing applications.

Haferkamp et al. [22] demonstrated a positive correlation between circularity and powder layer density, highlighting the importance of particle morphology for achieving stable process conditions and high-density components. The mean circularities exceed 0.7, which is commonly considered the minimum acceptable value for printable powders, since irregular particles below this range tend to increase interparticle friction, cohesion, and agglomeration phenomena, ultimately reducing powder flowability and layer uniformity [18]. Powders with circularity values above 0.80 generally demonstrate significantly better rheological behavior and spreading performance, especially in LPBF systems. DED

technologies can tolerate lower morphological regularity than LPBF processes because they are less sensitive to powder spreading defects. Highly spherical particles still provide significant advantages, including improved carrier-gas entrainment, more stable powder streams, and higher deposition efficiency [23].

The mean circularity values exceeded 0.7, a value generally considered indicative of powders with acceptable flowability for many additive manufacturing applications.

This particle size classification could be useful to enable the produced powders to be tailored to the different 3D printing techniques. Indeed, the characteristics of the powder, especially particle size distribution, play a crucial role in 3D printing and, in particular, in the quality of the final product according to the specific additive manufacturing techniques. For instance, LPBF typically requires metal powders in the 10–45 μm range to promote high packing density and precise layer fusion, while powders in the 45–105 μm range are recommended for EBM systems [24].

The PSD analysis is given in Figure 4, where the raw material and the best test (7.9 kW, 3 slm carrier powder and 0.3 kg/h feeding rate) are compared with respect to volume distribution. Numerical PSD results also showed negligible particles with diameters under 20 μm, 3.3% in 20–45 μm, 88.1% in 45–106 μm, and 8.6% over 106 μm. Therefore, most of the powder is contained within the particle size range that exhibits the highest spheroidization degree.

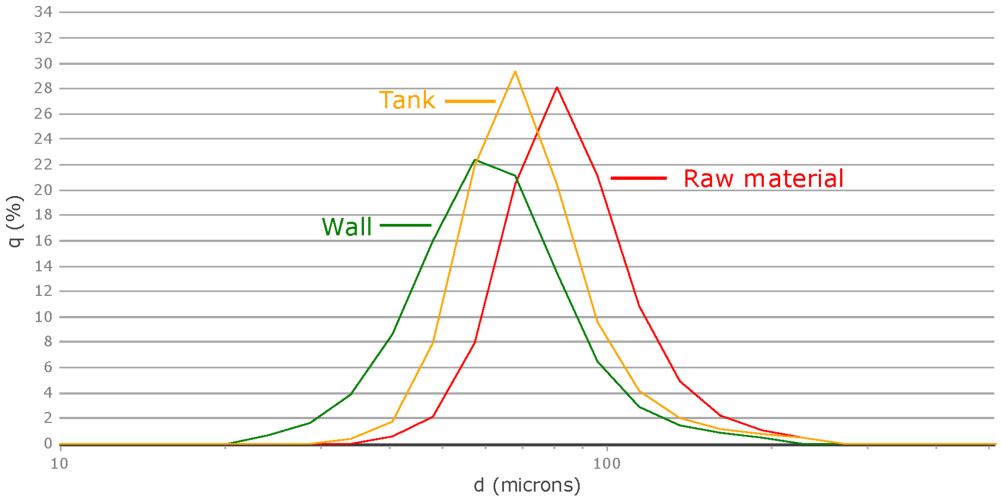


Figure 4. PSD of the raw material (red line) vs. samples in test C (wall and tank, green and yellow lines, respectively). Incremental volume percent (q) vs. diameter (d).

According to Thejane et al. [25], the average d_{90} of Ti6Al4V commercial powder is 35 μm for DMLs, 54 μm for Laser Curing and 92 μm for LENS. EBM typically employs gas-atomized powders with a controlled particle size distribution, generally characterized by d_{50} values in the range 45–70 μm and d_{90} approximately below 100 μm, in order to ensure adequate flowability and stable powder bed formation [26–28]. For these reasons, the PSD of the produced powder is appropriate for the processes mentioned, and it can be adjusted through sieving to meet the target specification range required for process optimization, while also considering particle morphology and the degree of spheroidization discussed above.

The powders were then characterized by XRD; the patterns of the samples before and after the plasma treatment are depicted in Figure 5.

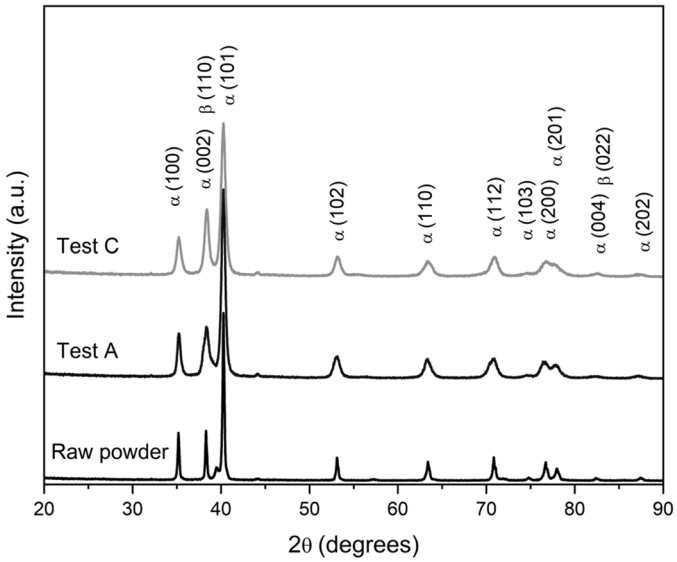


Figure 5. XRD patterns of the raw and plasma-processed powders at 12.2 kW (test A) and 7.9 kW (test C).

The raw A powder is predominantly characterized by the α-Ti phase, with only a weak diffraction peak at 2θ = 39.7° attributable to the β-Ti phase. Following plasma treatment, the powders retain the α-Ti phase, while the β-Ti (110) reflection appears less evident because of peak broadening, ultimately becoming undetectable.

The flowability of the produced powders in test C, after purification, was measured with the Hall Flow method and the obtained values are reported in Table 5.

Table 5. Hall Flow results for Ti6Al4V powder (before and after plasma treatment).

	HFR (s/50 g)	**Apparent Density (g/cc)**
Raw material	47.3	1.9
A test	35.8	2.2
C test	29.5	2.4
Commercial Powder OES (45–106 μm)	28.3–30.5	2.35–2.5

The raw material flows poorly (47.3 s/50 g) due to the irregular shape. After plasma treatment, the flow time drops dramatically to 29.5 s/50 g for the C test, which is nearly identical to the commercial powder benchmark. Additionally, the apparent density increases because the spherical particles pack more tightly, ensuring uniform powder bed layering [29]. Therefore, the test at 7.9 kW successfully improves the physical and flow characteristics of irregular Ti6Al4V raw powder, making it comparable to commercial powders for AM.

The chemical composition of Ti6Al4V powders is shown in Table 6.

The plasma treatment leads to an increase in the oxygen, nitrogen, and hydrogen contents compared to the raw material. These results suggest that the plasma processing conditions suffer little contamination from the atmospheric and process gases, likely associated with residual oxygen and moisture or minor air ingress into the processing environment. Although the measured impurity levels remain relatively low compared to other experimental studies in the literature [13], these findings highlight the importance of improving the atmospheric control during plasma processing to minimize oxygen, nitrogen, and hydrogen incorporation and thereby preserving the chemical integrity of

the powder. Alternatively, an appropriate post-processing cleaning or decontamination treatment could be implemented if further reduction in interstitial impurities is required for the desired application.

Table 6. Chemical composition results for Ti6Al4V powder (before and after plasma treatment).

	Oxygen (%)	Nitrogen (%)	Hydrogen (%)
Raw material	0.13	0.01	0.005
A test	0.28	0.21	0.059
C test	0.25	0.20	0.038
Commercial Powder Hoganas for AM OES (45–106 μm)	0.13	0.03–0.05	0.012

4. Conclusions

This study investigated the feasibility and effectiveness of using DC thermal plasma technology for the spheroidization of coarse, irregular Ti6Al4V feedstock powders within the 45–106 μm range. The experimental outcomes provided critical insights into both the morphological benefits and the chemical challenges associated with this processing route.

SEM images show spherical particles without satellites, with circularity above 0.7, a median particle size of approximately 65 μm and SPAN below 1. Therefore, DC thermal plasma treatment successfully converted the highly irregular raw material into high-circularity spherical particles. This significant morphological transformation reduced friction between particles, significantly improving powder flowability. Specifically, the flow time decreased significantly from an initial 47.3 s/50 g to an optimal 29.5 s/50 g, achieving a performance that directly matches commercial benchmarks (such as Höganäs for AM OES) and fulfills the rheological requirements for EBM systems.

Pre-treatment sieving was found to be the most effective strategy for enhancing spheroidization and powder quality. A classification of the produced powder proved useful for the further application of the powder in the 3d printing techniques. Powder characteristics, particularly particle size distribution, play a crucial role in additive manufacturing and directly dictate the final product quality. Consequently, the produced powder may be adapted for different AM technologies. However, further optimization of the atmospheric control during plasma processing and/or suitable post-processing treatments may be required to further reduce interstitial impurities according to the specific application requirements.

From the results of this study, it can be concluded that when the spheroidization process parameters of a DC plasma system are optimized for a particular powder feedstock consisting of irregular Ti6Al4V particles, particle morphology can be changed from irregular to spherical and PSD can be tailored to meet the requirements of a specific AM system.

Author Contributions: P.I.: Conceptualization, Validation, Investigation, Writing—Original Draft, Writing—Review & Editing; S.P.: Writing—Review and Editing, Visualization; C.B.: Investigation, Writing—Original Draft, Writing—Review and Editing; G.P.: Investigation; A.D.G.D.M.: Investigation; N.F.: Investigation; S.G.: Conceptualization, Validation, Investigation, Writing—Original Draft, Writing—Review and Editing, Supervision. All authors have read and agreed to the published version of the manuscript.

Funding: This work has been conducted within the framework of the three-year power system research plan "PTR2025-2027" program of the Italian Ministry of Environment and Energy Security (MASE)-ENEA, Project 1.4 ≪Materiali di Frontiera per Usi Energetici≫ and of the Research Project INSPIRATION (project code ARS01_00350) funded by the Italian Ministry of University and Research (MUR).

Institutional Review Board Statement: Not applicable.

Informed Consent Statement: Not applicable.

Data Availability Statement: The data that support the findings of this study are available within the article.

Conflicts of Interest: The authors declare no conflicts of interest.

References

1. Nguyen, H.D.; Pramanik, A.; Basak, A.K.; Dong, Y.; Prakash, C.; Debnath, S.; Shankar, S.; Jawahir, I.S.; Dixit, S.; Buddhi, D. A Critical Review on Additive Manufacturing of Ti-6Al-4V Alloy: Microstructure and Mechanical Properties. *J. Mater. Res. Technol.* **2022**, *18*, 4641–4661. [CrossRef]
2. Tshephe, T.S.; Akinwamide, S.O.; Olevsky, E.; Olubambi, P.A. Additive Manufacturing of Titanium-Based Alloys—A Review of Methods, Properties, Challenges, and Prospects. *Heliyon* **2022**, *8*, e09041. [CrossRef] [PubMed]
3. Jin, B.; Wang, Q.; Zhao, L.; Pan, A.; Ding, X.; Gao, W.; Song, Y.; Zhang, X. A Review of Additive Manufacturing Techniques and Post-Processing for High-Temperature Titanium Alloys. *Metals* **2023**, *13*, 1327. [CrossRef]
4. Dawes, J.; Bowerman, R.; Trepleton, R. Introduction to the Additive Manufacturing Powder Metallurgy Supply Chain: Exploring the Production and Supply of Metal Powders for AM Processes. *Johns. Matthey Technol. Rev.* **2015**, *59*, 243–256. [CrossRef]
5. DebRoy, T.; Wei, H.L.; Zuback, J.S.; Mukherjee, T.; Elmer, J.W.; Milewski, J.O.; Beese, A.M.; Wilson-Heid, A.; De, A.; Zhang, W. Additive Manufacturing of Metallic Components—Process, Structure and Properties. *Prog. Mater. Sci.* **2018**, *92*, 112–224. [CrossRef]
6. Sun, S.; Brandt, M.; Easton, M. Powder Bed Fusion Processes. In *Laser Additive Manufacturing*; Elsevier: Amsterdam, The Netherlands, 2017; pp. 55–77. [CrossRef]
7. Tobar, M.J.; Amado, J.M.; Montero, J.; Yáñez, A. A Study on the Effects of the Use of Gas or Water Atomized AISI 316L Steel Powder on the Corrosion Resistance of Laser Deposited Material. *Phys. Procedia* **2016**, *83*, 606–612. [CrossRef]
8. Sun, P.; Fang, Z.Z.; Zhang, Y.; Xia, Y. Review of the Methods for Production of Spherical Ti and Ti Alloy Powder. *JOM* **2017**, *69*, 1853–1860. [CrossRef]
9. Korzhyk, V.M.; Strohonov, D.V.; Tereshchenko, O.S.; Ganushchak, O.V.; Tunik, A.Y.; Kostin, V.A.; Chygileichyk, S.L.; Yuliuhin, V.K. Spherical Titanium Powder Production for 3D Printing by Plasma-Arc Atomization of Wire Materials. *Paton Weld. J.* **2025**, *2025*, 3–9. [CrossRef]
10. Cherezov, N.; Fadeev, A.; Samokhin, A.; Alymov, M. SHS-Hydrogenation, Thermal Dehydrogenation, and Plasma Spheroidization to Produce Spherical Titanium Powders from Titanium Sponge. *Alloys* **2024**, *3*, 246–256. [CrossRef]
11. Liu, M.; Huang, L.; Ren, C.; Wang, D.; Li, Q.; Li, J. Effect of Radiofrequency Plasma Spheroidization Treatment on the Laser Directed Energy Deposited Properties of Low-Cost Hydrogenated-Dehydrogenated Titanium Powder. *Materials* **2022**, *15*, 1548. [CrossRef] [PubMed]
12. Vert, R.; Pontone, R.; Dolbec, R.; Dionne, L.; Boulos, M.I. Induction Plasma Technology Applied to Powder Manufacturing: Example of Titanium-Based Materials. *Key Eng. Mater.* **2016**, *704*, 282–286. [CrossRef]
13. Nkhasi, N.; Du Preez, W.; Bissett, H. Plasma Spheroidisation of Irregular Ti6Al4V Powder for Powder Bed Fusion. *Metals* **2021**, *11*, 1763. [CrossRef]
14. Sheng, Y.-W.; Guo, Z.-M.; Hao, J.-J.; Yang, D.-H. Effect of Spheroidization of Ti–6Al–4 V Powder on Characteristics and Rheological Behaviors of Gelcasting Slurry. *Procedia Eng.* **2012**, *36*, 299–306. [CrossRef]
15. Xie, B.; Fan, Y.; Zhao, S. Characterization of Ti6Al4V Powders Produced by Different Methods for Selective Laser Melting. *Mater. Res. Express* **2021**, *8*, 076510. [CrossRef]
16. Huang, Q.; Huang, J.; Zhu, X.; Zhang, Y.; Cao, Y.; Liu, B.; Liu, Y.; Zhou, C. Ti-6Al-4V Powder with Extra Low Interstitial Element Fabricated Using Plasma Spheroidization and Hydrogen-Assisted Magnesium Deoxidation. *Chem. Phys. Lett.* **2026**, *882*, 142481. [CrossRef]
17. Iovane, P.; Borriello, C.; Pandolfi, G.; Portofino, S.; Rametta, G.; Tammaro, L.; Fedele, N.; Galvagno, S. Thermal Plasma Spheroidization and Characterization of Stainless Steel Powders Using Direct Current Plasma Technology. *Plasma* **2024**, *7*, 76–90. [CrossRef]
18. Cordova, L.; Campos, M.; Tinga, T. Revealing the Effects of Powder Reuse for Selective Laser Melting by Powder Characterization. *JOM* **2019**, *71*, 1062–1072. [CrossRef]
19. Korzhyk, V.; Strohonov, D.; Tereshchenko, O.; Peleshenko, S.; Ganushchak, O.; Demianov, O.; Li, Z.; Chen, Y. Application of DC Plasma Torches for Spheroidization Processes of Irregularly Shaped Powders. *AIMS Mater. Sci.* **2026**, *13*, 30–61. [CrossRef]
20. Ji, L.; Wang, C.; Wu, W.; Tan, C.; Wang, G.; Duan, X.-M. Spheroidization by Plasma Processing and Characterization of Stainless Steel Powder for 3D Printing. *Metall. Mater. Trans. A* **2017**, *48*, 4831–4841. [CrossRef]

21. Iovane, P.; Borriello, C.; Pandolfi, G.; Portofino, S.; De Girolamo Del Mauro, A.; Sico, G.; Tammaro, L.; Fedele, N.; Galvagno, S. Spheroidization of Alumina Powders for Additive Manufacturing Applications by DC Plasma Technology. *Molecules* **2025**, *30*, 453. [CrossRef] [PubMed]
22. Haferkamp, L.; Haudenschild, L.; Spierings, A.; Wegener, K.; Riener, K.; Ziegelmeier, S.; Leichtfried, G.J. The Influence of Particle Shape, Powder Flowability, and Powder Layer Density on Part Density in Laser Powder Bed Fusion. *Metals* **2021**, *11*, 418. [CrossRef]
23. Zhao, Y.; Cui, Y.; Hasebe, Y.; Bian, H.; Yamanaka, K.; Aoyagi, K.; Hagisawa, T.; Chiba, A. Controlling Factors Determining Flowability of Powders for Additive Manufacturing: A Combined Experimental and Simulation Study. *Powder Technol.* **2021**, *393*, 482–493. [CrossRef]
24. Popov, V.V.; Grilli, M.L.; Koptyug, A.; Jaworska, L.; Katz-Demyanetz, A.; Klobčar, D.; Balos, S.; Postolnyi, B.O.; Goel, S. Powder Bed Fusion Additive Manufacturing Using Critical Raw Materials: A Review. *Materials* **2021**, *14*, 909. [CrossRef] [PubMed]
25. Thejane, K.; Chikosha, S.; Du Preez, W. Characterisation and monitoring of TI6AL4V (ELI) powder used in different selective laser melting systems. *S. Afr. J. Ind. Eng.* **2017**, *28*, 161–171. [CrossRef]
26. Murr, L.E.; Gaytan, S.M.; Medina, F.; Martinez, E.; Martinez, J.L.; Hernandez, D.H.; Machado, B.I.; Ramirez, D.A.; Wicker, R.B. Characterization of Ti–6Al–4V Open Cellular Foams Fabricated by Additive Manufacturing Using Electron Beam Melting. *Mater. Sci. Eng. A* **2010**, *527*, 1861–1868. [CrossRef]
27. Antonysamy, A.A.; Parimi, L.L.; Mani, M.K.; Schade, C.T.; Lunt, A.J.G. Powder Characterisation and the Impact on Part Performance in Electron Beam Melted Ti6Al4V. *Mater. Des.* **2024**, *239*, 112788. [CrossRef]
28. Galarraga, H.; Lados, D.A.; Dehoff, R.R.; Kirka, M.M.; Nandwana, P. Effects of the Microstructure and Porosity on Properties of Ti-6Al-4V ELI Alloy Fabricated by Electron Beam Melting (EBM). *Addit. Manuf.* **2016**, *10*, 47–57. [CrossRef]
29. Hao, Z.; Chen, Y.; Zhang, Q.; Wang, P.; Shu, Y.; He, J. Fabrication of Spherical Ti-6Al-4V Powder by RF Plasma Spheroidization Combined with Mechanical Alloying and Spray Granulation. *Adv. Powder Technol.* **2022**, *33*, 103379. [CrossRef]

Disclaimer/Publisher's Note: The statements, opinions and data contained in all publications are solely those of the individual author(s) and contributor(s) and not of MDPI and/or the editor(s). MDPI and/or the editor(s) disclaim responsibility for any injury to people or property resulting from any ideas, methods, instructions or products referred to in the content.